ACKNOWLEDGMENT

Acknowledgment is owed to Dr. D. H. Steinbrecher for introduction to the concept of the use of impedance transformation for the predetermination of reflection characteristics in switching. M. L. Smith is thanked for discussions of the analytical aspects of the derivation.

REFERENCES

[1] B. E. Dobratz, N. J. Ho, G. H. Lee, and H. T. Suyematsu, "Microwave analog and digital signal processors," *Proc. IEEE Int. Solid State Circuits Conf.*, pp. 76–77, 1978.
[2] J. M. Robinson and A. Husain, "Design of direct phase modulators for high speed digital radio systems using MIC techniques," in *Proc. IEEE MTT-S Int. Symp. Dig.*, pp. 220–223, 1977.
[3] J. F. White, "Diode phase shifters for array antennas," *IEEE Trans. Microwave Theory Tech.*, vol. MTT-22, pp. 658–674, June 1974.
[4] B. Glance, "A fast low-loss microstrip PIN phase shifter," *IEEE Trans. Microwave Theory Tech.*, vol. MTT-27, pp. 14–16, Jan. 1979.
[5] H. Junghaus, "A Ku-band hybrid-coupled 4-phase modulator in MIC technology," in *Trans. European Microwave Conf.* (Hamburg, Germany), pp. 133–137, 1975.
[6] T. Yahara, Y. Kadomaki, H. Hoshika, and K. Shirahata, "Broadband 180° phase shift section in X-band," *IEEE Trans. Microwave Theory Tech.*, vol. MTT-23, pp. 307–309, Mar. 1975.
[7] K. Hirai and S. Kamihashi, "Practical design of C-band MIC PIN phase shifters," in *Proc. IEEE MTT-S Int. Symp. Dig.*, pp. 229–231, 1979.
[8] H. Atwater, "Reflection coefficient transformation for phase-shift circuits," *IEEE Trans. Microwave Theory Tech.*, vol. MTT-28, pp. 563–568, June 1980.
[9] S. Kawakami, "Figure of merit associated with variable-parameter one-port for R.F. switching and modulation," *IEEE Trans. Circuit Theory*, vol. CT-12, pp. 321–328, Sept. 1965.
[10] K. Kurokawa and W. O. Schlosser, "Quality factor of switching diodes for digital modulation," *IEEE Trans. Microwave Theory. Tech.*, vol. MTT-18, pp. 180–181, Jan. 1970.

Analysis of Open-Type Dielectric Waveguides by the Finite-Element Iterative Method

MASATOSHI IKEUCHI, HIDEO SAWAMI, AND HIROSHI NIKI

Abstract—**Dispersion characteristics for open-type dielectric waveguide structures operated at millimeter-and submillimeter-wave frequencies are calculated by a finite-element iterative procedure with a given criterion on the maximum field strength at the virtual boundary. Numerical results for a rectangular dielectric image guide are presented and compared with results from other methods. The strip dielectric guide and the insulated image guide with finite-or infinite-width substrates are also analyzed.**

I. INTRODUCTION

VARIOUS dielectric waveguide structures operated at millimeter-and submillimeter-wave frequencies have been recently developed [1]–[3]. In the structure design, it becomes important to calculate the dispersion characteristics, the field distributions, and other quantities. However, rigorous solutions have not been known except for specific structures [4]. Many approximate and numerical methods [1]–[10] for analyzing the various structures (see Fig. 1.) have been presented in the past decade. Among them, the effective dielectric constant method [1], [2], the transverse resonance method [5], [6], and other methods [3], [7] which cannot provide complete information on the field distributions, and it has been recently suggested [8] that [1], [2] are the single-mode approximations. The field-matching method [9] and the method employing the telegraphist's equation [10] are efficient where metallic walls are assumed. The influence of the metallic wall on the inherent

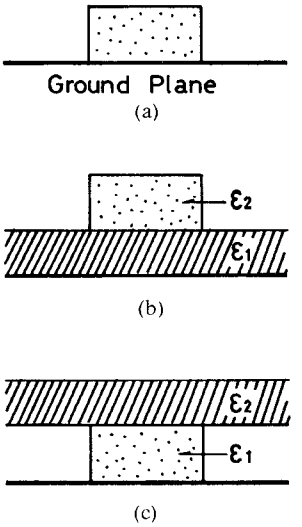

Fig. 1. Dielectric waveguide structures with conducting ground plane. (a) Dielectric image guide. (b) Strip dielectric guide for $\epsilon_1 > \epsilon_2$, insulated image guide for $\epsilon_1 < \epsilon_2$, single-material guide for $\epsilon_1 = \epsilon_2$. (c) Inverted strip dielectric guide for $\epsilon_1 \leqslant \epsilon_2$

Manuscript received July 28, 1980; revised October 29, 1980.
The authors are with the Department of Applied Mathematics, Okayama University of Science, Okayama, 700 Japan.

0018-9480/81/0300-0234$00.75 ©1981 IEEE

characteristics is not rigorously and systematically discussed in the mode-matching method [8] as well as [9], [10]. On the other hand, the finite-element method (e.g., [11], [12]) has been applied to dielectric waveguide structures enclosed by metallic walls. It is not easy to treat the open-type structure involving inhomogeneous dielectric media, except for the so-called quasi-static approximation [13], [14]. Boundary elements [15] have been recently developed for open-type structures, but an empirical parameter is introduced and the variational formula [16] for the close-type structure is employed.

In this paper, a finite-element iterative method based on shifting the bounded region for analysis to satisfy a given criterion at a virtual boundary is presented. The virtual boundary is mathematically and physically chosen to enclose the open-type dielectric waveguide structure. An E_z–H_z variational formulation [16]–[18] is employed. In the present method, the influence of the virtual boundary on the dispersion characteristics and the field distributions can be predicted, and thus solutions with desired accuracies can be systematically obtained.

II. Finite-Element Iterative Method

A. Variational Formulation

Assume the dielectric waveguide structure to be uniform, with isotropic, loss-free media, as shown in Fig. 2. The bounded region $S(R)(=\Omega_1 \cup \Omega_2)$ for analysis is separated from the unbounded region by the virtual boundary $\Gamma(R)$. Ω_1 denotes the core with the maximum radius $r(<R)$. The propagating modes can be expressed as a combination of the TE and TM modes. The E_z–H_z variational formula [17], [18] for the electromagnetic field in $S(R)$ is known to be

$$J_0=\int_{S(R)}\int \nabla u^T L \nabla u\, dS-\int_D u^T M(\partial u/\partial s)\, ds-k_0^2\int_{S(R)}\int u^T N u\, dS-J_e \tag{1}$$

where the field is assumed to have the dependence $e^{j\omega t}$ with the angular frequency ω. Also, the symbols are

u $=[\phi,\psi]^T=[H_z,(\omega\epsilon_0/\beta)E_z]^T$,
E_z, H_z axial components,
∇ gradient operator,
D internal boundary of Ω_1 and Ω_2,
s tangential unit vector to $\Gamma(R)$,
β propagation constant,
k_0^2 $=(\omega/c)^2(1-\epsilon_e)$,
ϵ_e $=(\beta c/\omega)^2$ effective dielectric constant,
c $=1/\sqrt{\epsilon_0\mu_0}$ light velocity in vacuum,
τ $=(1-\epsilon_e)/(\epsilon_r-\epsilon_e)$ coupling parameter,
ϵ_r relative dielectric constant,
L $=\tau N$,

$$M=\begin{bmatrix}0 & \tau\epsilon_e\\ -\tau\epsilon_e & 0\end{bmatrix},$$

$$N=\begin{bmatrix}1 & 0\\ 0 & \epsilon_e\epsilon_r\end{bmatrix}.$$

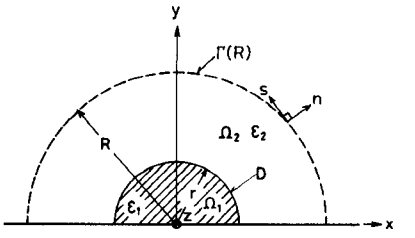

Fig. 2. Geometry of the problem. $\epsilon_i=\epsilon_{ri}\epsilon_0$, $\epsilon_1>\epsilon_2\geq\epsilon_0$, ϵ_0 is permittivity in vacuum and $\Gamma(R)$ is the virtual boundary.

The last term in the right-hand side of (1) is

$$J_e=j\int_{\Gamma(R)} u^T K v\, ds \tag{2}$$

where

v $=[\xi,\eta]^T=[H_s,(\omega\epsilon_0/\beta)E_s]^T$,
E_s, H_s tangential components,
K $=(k_0^2/\tau\beta)M$.

Here, (2) denotes the Poynting's power flow in the outward normal direction n, through $\Gamma(R)$. Note that (1) is not defined for $\omega=0$ and/or $\beta=0$. Now J_e becomes zero when the distance R is infinite, or when both ϕ and ψ are zero at $\Gamma(R)$. In other words, ϕ should be forced to be zero at $\Gamma(R)$ when ψ is assumed to be zero. Therefore, for the bounded region $S(R)$, the authors present the following constrained extremal problem: extremize the variational formula

$$J=J_0+J_e \tag{3}$$

with respect to u with the constraint

$$\psi(x,y)=0, \qquad \text{for } (x,y)\in\Gamma(R) \tag{4}$$

and such that the quantity

$$I(R)=20\log\left[\max_{(x,y)\in\Gamma(R)}|\phi(x,y)|\Big/\max_{(x,y)\in S(R)}|u(x,y)|\right] \tag{5}$$

is minimized. Here, $I(R)$ represents the normalized maximum field strength at $\Gamma(R)$, and J approaches J_0 for $I(R)\to-\infty$. Then $\phi(x,y)\to 0$ and $\partial\phi(x,y)/\partial n\to 0$ ($(x,y)\in\Gamma(R)$), and $J_e\to 0$. Thus $I(R)$ physically means the magnitude of the Poynting's power flow J_e through $\Gamma(R)$. The minimization of $I(R)$ is possible since $\phi(x,y)$ ($(x,y)\in\Gamma(R)$) does not become zero for finite R excepting the case of the complete TM-mode propagation, and since u and v are exponentially damping with respect to $R(>r)$.

B. Finite-Element Formulation

For the nth finite distance R_n, the bounded region $S(R_n)=S_n$ enclosed by $\Gamma(R_n)=\Gamma_n$ is consistently sub-

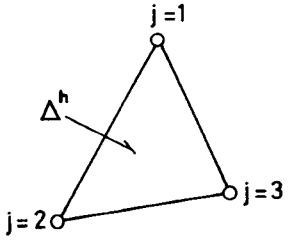

Fig. 3. Triangular element Δ^h. $j(=1,2,3)$ denotes the node number.

divided [18] into triangular elements Δ^h (see Fig. 3.) Here, the subscript $n(\geq 1)$ corresponds to the iteration number. The axial components $u=[\phi, \psi]^T$ are approximated over Δ^h in the usual way, as

$$u \simeq \begin{bmatrix} \phi^n \\ \psi^n \end{bmatrix} = \begin{bmatrix} \Sigma_{j=1}^{3} \phi_j^n f_j(x, y) \\ \Sigma_{j=1}^{3} \psi_j^n f_j(x, y) \end{bmatrix} \tag{6}$$

where $u_e^n = [\{\phi_j^n\}, \{\psi_j^n\}]^T$ is the unknown element vector and $\{f_j(x, y)\}$ is the linear interpolating function [18]. Substituting (6) into (3) and extremizing it with respect to u_e^n, the following element matrix equation is derived:

$$\partial J/\partial u_e^n = \left[\begin{array}{c|c} \tau A & \tau \epsilon_e C \\ \hline -\tau \epsilon_e C & \tau \epsilon_e \epsilon_r A \end{array}\right] u_e^n - k_0^2 \left[\begin{array}{c|c} B & 0 \\ \hline 0 & \epsilon_e \epsilon_r B \end{array}\right] u_e^n + j(\epsilon_e k_0^2/\beta) w_e^n = 0 \tag{7}$$

where for $i, j = 1,2,3$

$$\left.\begin{aligned} A_{ij} &= \int\int_{\Delta^h} \nabla f_i \nabla f_j \, dS, \qquad B_{ij} = \int\int_{\Delta^h} f_i f_j \, dS, \\ C_{ij} &= \int_{\Delta^h D} f_i (\partial f_j/\partial s) \, ds, \quad \text{and } w_e^n = \int_{\Delta^h \Gamma_n} f_i v_e^n \, ds \end{aligned}\right\}. \tag{8}$$

Here, v_e^n is the finite-element approximation to the tangential components $[\eta, -\xi]^T$, and $\Delta^h D$, $\Delta^h \Gamma_n$ denote the discretized internal and virtual boundaries for Δ^h, respectively. A, B, and $C(=-C^T)$ are known as the element stiffness, mass, and coupling matrices, respectively. Note that C is generated only for the tangential element to D, as seen from the third equation in (8). The load vector w_e^n is not required to be generated in practice, because of the criterion (10) described below. Assume that u^n is the unknown global vector generated by assembling all u_e^n over S_n. Then (5) can be approximated as

$$I(R_n) \simeq -\delta_n = 20 \log [\| u_\Gamma^n \| / \| u^n \|] \tag{9}$$

where $\| \cdot \|$ denotes the maximum norm and u_Γ^n stands for the nodal values at Γ_n. Instead of minimizing (5), the following criterion is presented:

$$\delta_n \geq \delta \tag{10}$$

where δ is given as a large positive number. Here, $-\delta$ means the upper limit for $I(R)$, and thus the magnitude of J_e is approximately proportional to $e^{-\delta/10}$. Therefore, the influence of $\Gamma(R)$ on the dispersion characteristics and other quantities can be predicted by (10). From (7) and (10) the following global matrix equation is derived:

$$G_n u^n = k_0^2 H_n u^n \tag{11}$$

where G_n and H_n are real, symmetric matrices and u^n is forced to satisfy (4). In the practical computations, (11) is first solved for the initial bounded region $S_1(n=1)$ at the fixed, large $\epsilon_e (1 \leq \epsilon_e \leq \max \epsilon_r)$, where S_1 is chosen to be slightly larger than the core Ω_1 since the surface waves concentrate in Ω_1 at the high frequencies. If the solution u^1 at the first stage is satisfied by (10), then (11) is successively solved for S_1 at the fixed, smaller ϵ_e. Otherwise, the second bounded region S_2 is next chosen, where $S_n \supset S_{n-1} \cdots \supset S_1$, and the computations are repeated until u^n satisfies (10). It is suggested that the iteration number $n=2$ or 3 at most. As a result, the solutions $k(=\omega/c)$ and u^n with the desired accuracies will be obtained over the wide range of ϵ_e (or $\beta c/\omega$), except for nonphysical, spurious solutions [17],[18],[20],[21] (see Section III-C). Note that the spurious solutions occur in slow-wave region ($\epsilon_e > 1$) [18],[21].

III. Numerical Results

A. Rectangular Dielectric Image Guide

Fig. 4 shows the bounded region $S_n(n=1,2,\cdots)$ for analysis and the subdivisions into elements. Fig. 5 shows the normalized field strength F_n in the vertical direction. Here, F_n asymptotically approaches F_∞ shown by the broken line, as the iteration number n is increasing, or as S_n is extending. Then F_∞ will be the field strength for the unbounded problem. In Fig. 6, the behavior of the computed wavenumber $ka(=\omega a/c)$ at the nth stage is shown for the distance R_n, where the broken line denotes the extrapolated value obtained by the Aitken's formula [19]. It is obvious that the convergence of ka depends on both R_n and the normalized propagation constant $\beta c/\omega$. Therefore, in order to obtain solutions with desired accuracies the virtual boundary Γ_n should be systematically shifted according to criterion (10), as described in Section II. Indeed, it is found from Fig. 7 that the relative error e of the computed ka uniformly decreases over the wide range of $\beta c/\omega$ as n is increasing. Also, the relative error e uniquely relates to δ_n, bounded by the given δ. Note that the extrapolated ka is identified with the rigorous solution. Here, e implies the influence of both the virtual boundary Γ_n and the finite-element approximation, and, it is estimated to be less than 1.00 and 0.01 percent for $\delta = 10$, 20, respectively. Fig. 8 shows the dispersion curve for the rectangular dielectric image guide obtained by the present method, where $\delta = 8$ and the maximum value of e is estimated to be less than 2.00 percent. The result obtained by the method of [10] can be seen to be very much influenced over $1.0 \leq \beta c/\omega \leq 1.2$ by the metallic walls.

B. Strip Dielectric Guide and Insulated Image Guide

The present method is also applicable to dielectric waveguide structures involving multidielectric layers. For exam-

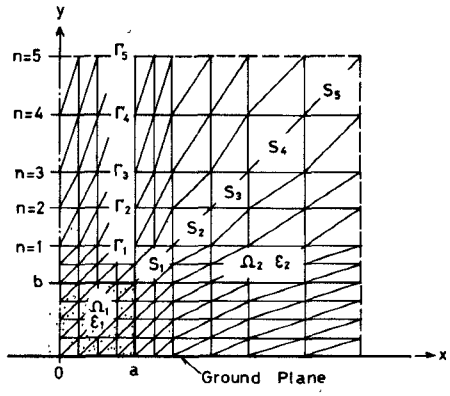

Fig. 4. Bounded region S_n for analysis enclosed by virtual boundary Γ_n and conducting ground plane, and the subdivision into elements. $a=b=5.0$ mm, $\epsilon_{r1}=2.5$, $\epsilon_{r2}=1.0$, and n denotes the iteration number.

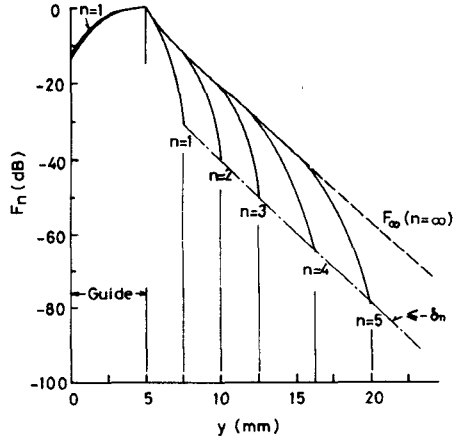

Fig. 5. Behavior of normalized field strength F_n as a function of both the vertical distance and the iteration number. $\beta c/\omega = 1.400$, $c=1/\sqrt{\epsilon_0\mu_0}$ is light velocity in vacuum, and δ_n is given by (9).

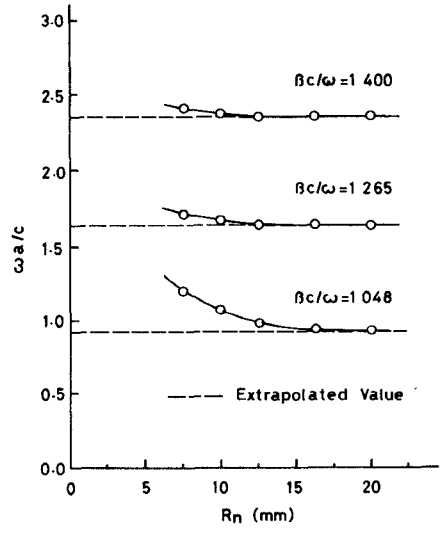

Fig. 6. Convergence of normalized frequencies. --- denotes the extrapolated value by Aitken's formula [19].

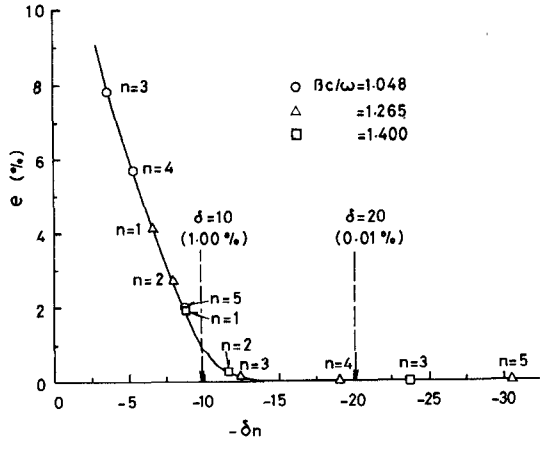

Fig. 7. Relation of the relative error of computed frequencies and the maximum field strength at virtual boundary. δ is given in (10).

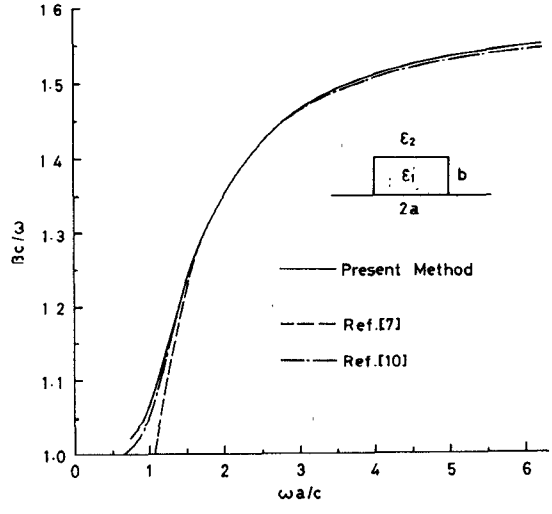

Fig. 8. Dispersion characteristics of the E_{11}^{y} mode in dielectric image guide. $a=b=5.0$ mm, $\epsilon_{r1}=2.5$, $\epsilon_{r2}=1.0$, $\delta=8$.

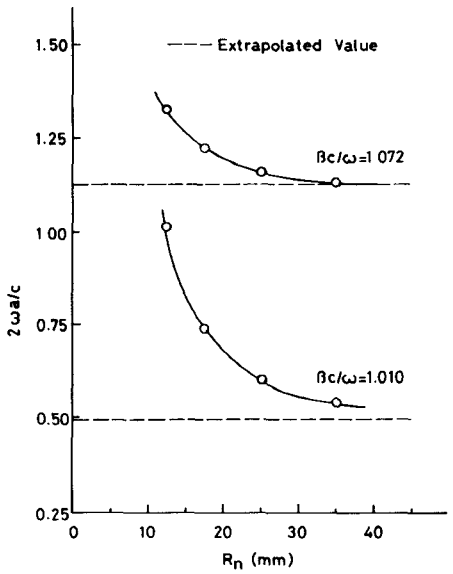

Fig. 9. Convergence of normalized frequencies. Insulated image guide (see Fig. 10.) $a=d_1=d_2=5.0$ mm, $b=10.0$ mm, $\epsilon_{r1}=2.55$, $\epsilon_{r2}=2.62$.

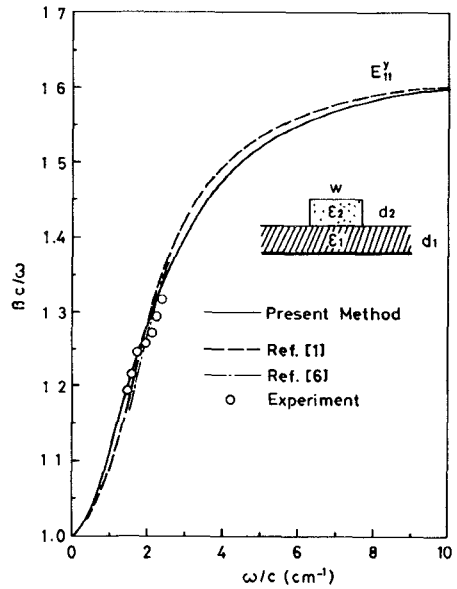

Fig. 11. Comparison of the present method with other methods for the strip dielectric guide. $w=0.65$ cm, $d_1=0.50$ cm, $d_2=0.32$ cm, $\epsilon_{r1}=2.62$, $\epsilon_{r2}=2.55$, $\delta=6$.

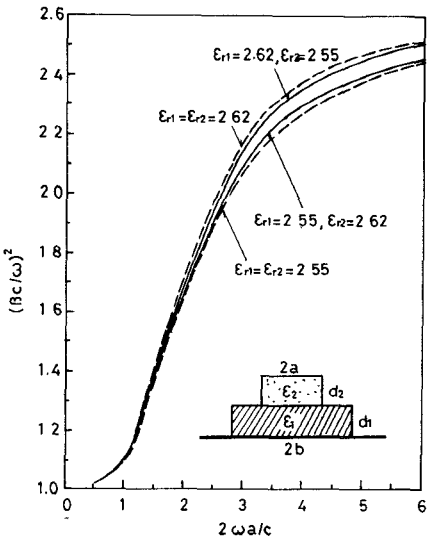

Fig. 10. Dispersion characteristics of the E_{11}^y mode in strip dielectric guide and insulated image guide. ---: single-material guide, $a=d_1=d_2=5.0$ mm, $b=10.0$ mm, $\delta=8$.

ple, similar results to Figs. 6 and 7 for the rectangular dielectric image guide are obtained for the insulated image guide, as shown in Fig. 9. Fig. 10 shows the dispersion curves for the strip dielectric guide ($\epsilon_1>\epsilon_2>\epsilon_3=\epsilon_0$), the insulated image guide ($\epsilon_3<\epsilon_1<\epsilon_2$), and the single-material guide ($\epsilon_1=\epsilon_2>\epsilon_3$) with finite-width ($2b$) substrates. Here, the results are systematically calculated by setting $\delta=8$ to the criterion (10), and then the maximum error of the solution $2ka$ is estimated to be about 2.00 percent from the results in Figs. 6, 7, and 9. The dispersion curves for the strip dielectric guide and the insulated image guide separately approach to the ones for the two different single-material guides at high frequencies. Fig. 11 shows the dispersion curve for the strip dielectric guide with infinite-width substrate, where $\delta=6$ is set and the maximum error of $k(=\omega/c)$ is estimated to be about 5.0 percent. Here, the solid line is, on the whole, different from the results obtained by the other methods [1], [6], but better agreement will be attained by setting δ larger. In the strip dielectric guide and the insulated image guide, the fields penetrate into the dielectric strip and substrate, respectively, when the difference between ϵ_1 and ϵ_2 is small. At high frequencies, the maximum energy in the insulated image guide is located at the center of the dielectric strip, and the fields are very similar to the ones in the rectangular dielectric image guide. Therefore, the insulated image guide with finite-width substrate should be operated at high frequencies. Note that the guiding mechanism has been numerically discussed in [10] for dielectric waveguide structures with infinite-width substrates.

C. Computational Remarks

In the present method, the Householder's method, the Cholesky method, and the method of bisections are suitably used for solving (11), and the method of inverse iterations is used for calculating (9). The finite-element solutions in the E_z–H_z variational formulation have been known to include nonphysical, spurious solutions [17],[18],[20],[21]. In order to avoid confusion, such spurious solutions are not shown in Figs. 8, 10, and 11. For example, in Fig. 12 the spurious modes and the physical, high-order modes are shown for the strip dielectric guide with finite-width substrate. The spurious solutions appear to behave as the physical, nondispersive surface waves, but they may be separated from the physical modes by observing the dispersion curves. Here, the dispersion curves of the high-order modes are calculated by applying (10) for the first mode, and then they may be worse in the accuracies than the dispersion curve of the first mode. The

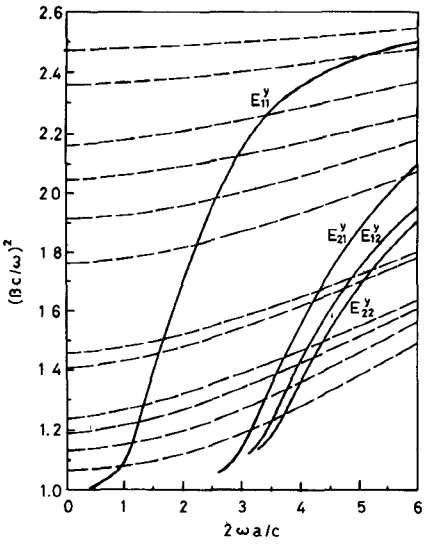

Fig. 12. Dispersion characteristics of a number of modes in the strip dielectric guide (see Fig. 10). —: physical modes, ---: spurious modes, $a=d_1=d_2=5.0$ mm, $b=10.0$ mm, $\epsilon_{r1}=2.62$, $\epsilon_{r2}=2.55$, $\delta=8$.

dispersion curves can be improved by applying (10) for the desired high-order modes. Note that dielectric waveguide structures for millimeter waves are usually required to work in a single mode.

IV. Conclusion

In this paper, a finite-element iterative method for analyzing open-type dielectric waveguide structures is presented. The wavenumbers, field distributions, and other quantities are systematically obtained by shifting the virtual boundary Γ_n and iteratively calculating the field strength until the criterion (10) is satisfied. As a result, dispersion curves with desired accuracies are calculated over a wide range of the propagation constant β, and also they can be improved by setting δ larger. In this sense, the present method is a practical approach to the error estimation of finite-element solutions in unbounded problem. The method is easily applicable to various structures, as shown in the analysis of the strip dielectric guide with finite-or infinite-width substrate and the others. In addition, the solutions can be improved by employing high-order elements. In this case, the element matrix equation is expressed as (7) and (8). The method may be applicable to optical dielectric waveguides without conducting ground planes. In order to improve the solutions at frequencies close to cutoffs, the bounded regions S_n for analysis are required to be extended, and then the large global matrix equations (11) must be solved. The authors will discuss this problem in their future work.

References

[1] W. McLevige, T. Itoh, and R. Mittra, "New waveguide structures for millimeter-wave and optical integrated circuits," *IEEE Trans. Microwave Theory Tech.*, vol. MTT-23, pp. 788–794, Oct. 1975.

[2] T. Itoh, "Inverted strip dielectric waveguide for millimeter-wave integrated circuits," *IEEE Trans. Microwave Theory Tech.*, vol. MTT-24, pp. 821–827, Nov. 1976.

[3] E. A. J. Marcatili, "Slab-coupled waveguides," *Bell Syst. Tech. J.*, vol. 53, pp. 645–674, Apr. 1974.

[4] W. Schlosser and H. G. Unger, "Partially filled waveguides and surface waveguides of rectangular cross section" in *Advances in Microwaves*, vol. 1, L. Young, Ed. New York: Academic Press, 1966, pp. 319–387.

[5] S. T. Peng and A. A. Oliner, "Leakage and resonance effects on strip waveguides for integrated optics," *Trans. Inst. Electron. Commun. Eng. Japan*, vol. 61-E, pp. 151–154, Mar. 1978.

[6] M. Koshiba and M. Suzuki, "Microwave network analysis of dielectric waveguides for millimeter waves made of dielectric strip and planar dielectric layer," *Trans. Inst. Electron. Commun. Eng. Japan*, vol. 63-E, pp. 344–350, May 1980.

[7] E. A. J. Marcatili, "Dielectric rectangular waveguide and directional coupler for integrated optics," *Bell Syst. Tech. J.*, vol. 48, pp. 2079–2102, Sep. 1969.

[8] R. Mittra, Y. L. Hou, and V. Jamnejad, "Analysis of open dielectric waveguides using mode-matching technique and variational methods," *IEEE Trans. Microwave Theory Tech.*, vol. MTT-28, pp. 36–43, Jan. 1980.

[9] K. Solbach and I. Wolff, "The electromagnetic fields and the phase constants of dielectric image lines," *IEEE Trans. Microwave Theory Tech.*, vol. MTT-26, pp. 266–274, Apr. 1978.

[10] K. Ogusu, "Numerical analysis of the rectangular dielectric waveguide and its modifications," *IEEE Trans. Microwave Theory Tech.*, vol. MTT-25, pp. 874–885, Nov. 1977.

[11] M. Ikeuchi, K. Inoue, H. Sawami, and H. Niki, "Finite-element analysis of the coplanar-type striplines," *Trans. Inst. Electron. Commun. Eng. Japan*, vol. 61-B, pp. 421–423, May 1978.

[12] C. Yeh, S. B. Dong, and W. Oliver, "Arbitrarily shaped inhomogeneous optical fiber or integrated optical waveguides," *J. Appl. Phys.*, vol. 46, pp. 2125–2129, May 1975.

[13] Z. J. Csendes, "A note on the finite-element solution of exterior-field problems," *IEEE Trans. Microwave Theory Tech.*, vol. MTT-24, pp. 468–473, July 1976.

[14] B. H. McDonald and A. Wexler, "Finite-element solution of unbounded field problems," *IEEE Trans. Microwave Theory Tech.*, vol. MTT-20, pp. 841–847, Dec. 1972.

[15] C. Yeh, K. Ha, S. B. Dong, and W. P. Brown, "Single-mode optical waveguides," *Appl. Opt.*, vol. 18, pp. 1490–1504, May 1979.

[16] P. Daly, "Hybrid-mode analysis of microstrip by finite-element methods," *IEEE Trans. Microwave Theory Tech.*, vol. MTT-19, pp. 19–25, Jan. 1971.

[17] Z. J. Csendes and P. Silvester, "Numerical solution of dielectric loaded waveguides: I. Finite-element analysis," *IEEE Trans. Microwave Theory Tech.*, vol. MTT-18, pp. 1124–1131, Dec. 1970.

[18] M. Ikeuchi, K. Inoue, H. Sawami, and H. Niki, "Spurious solutions in the finite-element analysis of microstrip lines," *Trans. Inst. Elec. Eng. Japan*, vol. 98(A), pp. 415–422, Aug. 1978.

[19] C. E. Fröberg, *Introduction to Numerical Analysis*. Reading, MA: Addison-Wesley, 1965, pp. 185–186.

[20] A. Konrad, "Vector variational formulation of electromagnetic fields in anisotropic media," *IEEE Trans. Microwave Theory Tech.*, vol. MTT-24, pp. 553–559, Sep. 1976.

[21] Z. J. Csendes, "The high-order polynomial finite element method in electromagnetic field computation," in *Finite Elements in Electrical and Magnetic Field Problems*, M. V. K. Chari and P. P. Silvester, Eds. Chichester, England: Wiley, 1980, pp. 125–143.